The electronic structure of liquid alkali metals: calculation of photoemission spectra. II. The heavy alkali metals K, Rb, and Cs

1991 J. Phys.: Condens. Matter 3 6947

(http://iopscience.iop.org/0953-8984/3/35/024)

J. Phys.: Condens. Matter 3 (1991) 6947–6958. Printed in the UK

The electronic structure of liquid alkali metals: calculation of photoemission spectra: II. The heavy alkali metals K, Rb, and Cs

W Jank and J Hafner

Institut für Theoretische Physik, TU Wien, Wiedner Hauptstraße 8-10, A-1040 Wien, Austria

Received 25 February 1991

Abstract. Extending our recent investigation of the light liquid alkali metals (Jank W and Hafner J 1990 *J. Phys.: Condens. Matter* **2** 5065), we present first-principles calculations of the atomic structure, the electronic spectrum, and of the photoemission intensities of the heavy alkali metals K, Rb, and Cs in the molten state. We find that the width of the occupied band corresponds roughly to the prediction of the free-electron model. The shape of the densities of states, however, changes gradually from parabolic to triangular in the series Na–K–Rb–Cs, due to the incipient occupation of d states. In the photoemission spectra, this trend is enhanced by the dependence of the partial photoionization cross sections on the angular momentum and the binding energy of the emitted photoelectron, and of the energy of the incident photon.

1. Introduction

Recent progress in photoelectron spectroscopy from molten samples [1–4] has led to a renewal of interest in the electronic structure of liquid metals. In a series of recent publications the authors have demonstrated that accurate first-principles calculations of the electronic density of states (DOS) and of the photoemission intensites are now possible [5–9]. Investigations of the electronic properties of the liquid alkali metals, which constitute the testing area for all nearly free-electron (NFE) theories [10–11] are of special interest. Experimentally, it turns out that the energy distribution of the emitted photoelectrons is not of the parabolic form expected for NFE metals. In liquid Li one observes a substantial reduction of the band width W; in liquid Na W is close to the NFE prediction (as is also observed in polycrystalline Na [12]), but the shape of the spectrum is triangular rather than parabolic [3]. In our recent theoretical investigation of the atomic and electronic structures of liquid Li and Na [8] (hereafter this paper will be referred to as I) we have shown that the observed reduction of the band width of liquid Li results from a strong structure-induced 'Brillouin kink' in the DOS at an energy (in atomic units) of appoximately $(Q_p/2)^2$ above the bottom of the band (where Q_p is the wave vector corresponding to the main peak in the static structure factor). This is directly related to the strong p component in the non-local Li pseudopotential. In liquid Na the electronic DOS is quite close to the ideal NFE parabola, but the dependence of the partial photoionization cross sections $\sigma_l(E, \hbar\omega)$ on the angular momentum l and the binding energy E of the photoelectron, and on

0953-8984/91/356947+12$03.50

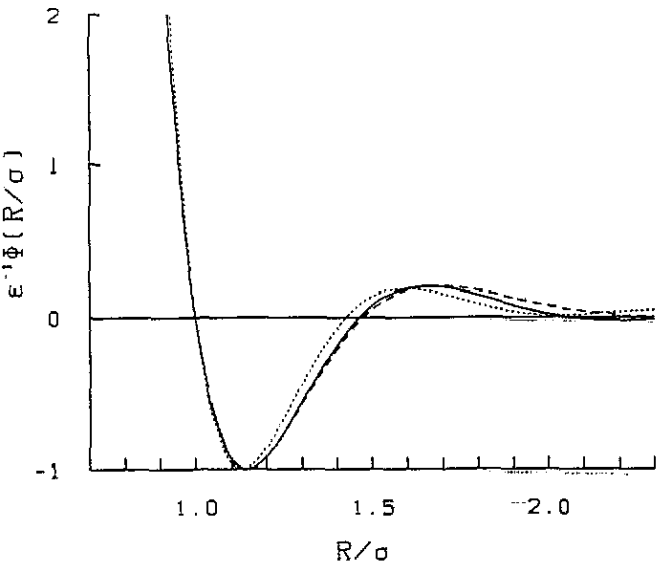

Figure 1. Scaled effective interatomic potentials $(1/\epsilon)\Phi(R/\sigma)$ (where σ is the smallest value of R for which $\Phi(R) = 0$ and ϵ is the magnitude of $\Phi(R)$ at its absolute minimum). Numerical values of ϵ and σ are given in table 2. Full line—K, dashed line—Rb, dotted line—Cs.

the energy $\hbar\omega$ of the photon lead to a triangular energy distribution of the emitted electrons, especially for photons in the ultraviolet energy range (UPS spectra).

In the present study we extend our investigations to the heavy alkali metals K, Rb, and Cs. It is well known that in the crystalline state the heavy alkali metals undergo a series of pressure-induced structural phase transitions [13–16]. It is generally accepted that the structural transformations result from a pressure-induced transfer of s and p electrons into d states [17–19]. The strong decrease of the transition pressure in the sequence K–Rb–Cs points to an increasing d-state occupation even under ambient presssure. In the liquid state, diffraction experiments on Cs under pressure demonstrate a transition from a soft-sphere-like structure to a more complicated atomic arrangement [20]. This would seem to indicate that a certain s–d electron transfer (increasing with pressure and atomic number) occurs also in the liquid metals.

Our investigations are based on the computational techniques described in detail in I and in [6], the main aspects are briefly recapitulated in section 2. The results are described in section 3. In both the crystalline and the liquid metals we find a peak in the electronic DOS at ~ 2 eV (K), ~ 1.5 eV (Rb), and ~ 1.2 eV (Cs) above the Fermi level, originating mainly from the d states. The lowering of the d peak accompanies an increasing transfer of electrons from p to d states, the total number of s electrons remaining essentially unchanged. Although the charge transferred is only of the order of a few hundreds of electrons per atom, the shape of the DOS is altered significantly: it is entirely triangular for liquid Rb and Cs. In the photoemission intensities, this trend is enhanced by the partial photoionization cross sections: in the sequence K–Rb–Cs the UPS spectra are increasingly dominated by the p- and d-electron contributions (especially at low photon energies). This results in a form of the UPS spectra tending from triangular in l-K to quadratic in l-Cs.

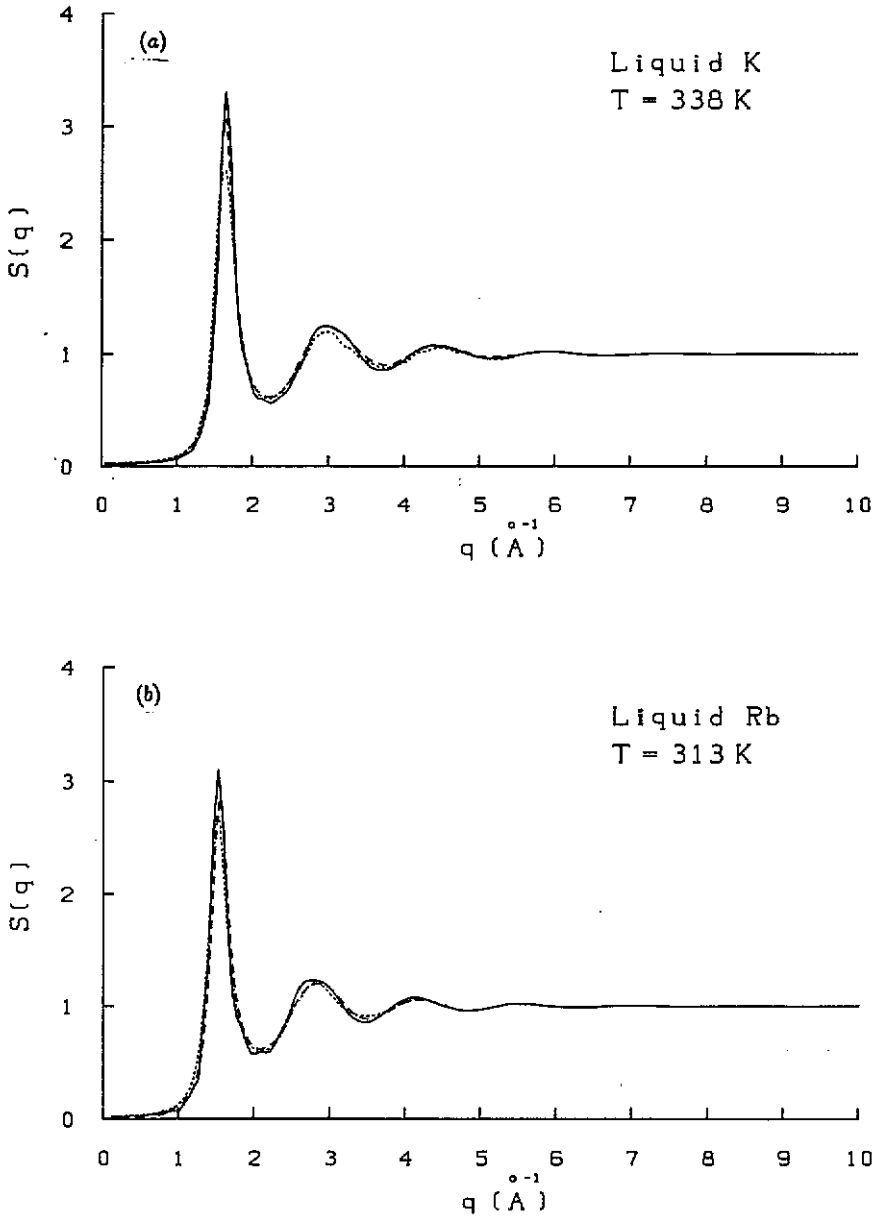

Figure 2. (*a*)–(*c*) Static structure factor of the heavy liquid alkali metals. Full line—molecular dynamics simulation. Diffraction data are shown for comparison: (*a*) K at $T = 338$ K. Dashed line—neutron diffraction, after Huijben *et al* [38]; dotted line—x-ray diffraction , after Waseda [39]. (*b*) Rb at $T = 313$ K, dashed line—neutron diffraction, after Copley end Lovesey [40], dotted line—x-ray diffraction, after Waseda [39]. (*c*) Cs at $T = 303$ K, dashed line—neutron diffraction, after Huijben et al [38], dotted line—x-ray diffraction, after Waseda [39].

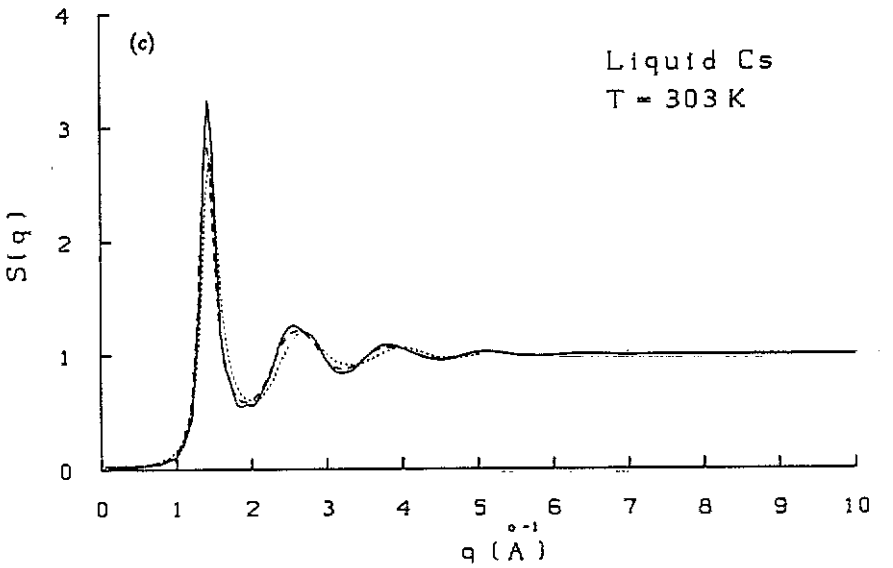

Figure 2. (Continued)

2. Calculational procedure

2.1. Interatomic forces

The effective interatomic potential is calculated using second-order pseudopotential perturbation theory [21,22]. To generate the ionic pseudopotential we use an orthogonalized plane-wave expansion of the conduction electron states and apply the optimization criterion of Cohen and Heine [23]. Local field corrections to the random phase dielectric function are treated in the Vashishta–Singwi and in the Ichimaru–Utsumi approximations [24,25], with only very small differences in the final results. The method is well documented in previous papers [26], where detailed applications to the calculation of structural energy differences and lattice vibrations of the crystalline metals are presented. Note that these calculations (like all other pseudopotential perturbation calculations) yield a stable hexagonal low-temperature phase for K, Rb, and Cs and predict a martensitic transformation to a body-centred cubic (BCC) phase at temperatures $T_M \leqslant 40$ K. On the other hand self-consistent total energy calculations based on linear-muffin-tin orbital techniques and norm-conserving pseudopotentials yield a stable BCC low-temperature phase, albeit with minimal structural energy differences [27,28]. This indicates that the structural stability is strongly correlated to the d-band occupancy. For a detailed review, see [29].

2.2. Liquid structure

The atomic structure of the liquid has been calculated using a microcanonical molecular dynamics simulation, based on a fifth-order predictor–corrector algorithm for the integration of the Newtonian equations of motion and an efficient net-cube technique for nearest-neighbour book-keeping [30,31]. For each element, two simulation runs were performed in parallel: one for a large ensemble with up to 2197 particles in the molecular dynamics cell for generating accurate liquid structure factors, and a second one with 64 atoms per cell for generating the atomic coordinates serving as

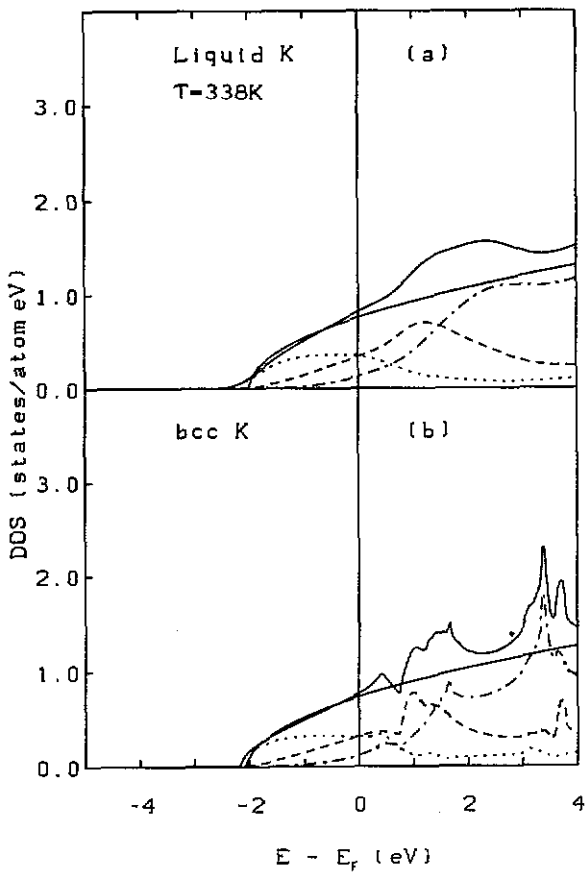

Figure 3. Electronic density of states in liquid K at $T = 338$ K (a) and in BCC K (b). Full line: total DOS, dotted line: partial DOS of s states, broken line: p states, dot-dashed line: d states. The free-electron parabola has been drawn for comparison.

the starting point of the electronic structure calculation. For the small cells we choose the largest cut-off for the interatomic potential compatible with the minimum-image convention ($R_{cut} \leqslant L/2$, where L is the cube edge of the MD cell); for the larger cell the potential was cut close to $R_{cut} \sim 10$ Å, always at the nearest node in the Friedel oscillations of the potential.

2.3. Electronic density of states

The electronic DOS was calculated using the linearized muffin-tin orbital (LMTO) version of the supercell approach [5–9], based on the scalar relativistic LMTO programs in the atomic sphere approximation [32,33]. For the heavy alkali metals a partial wave method such as the LMTO is preferred over a plane-wave expansion [34], because it converges more quickly for the resonant d states. In addition it produces directly the partial densities of states, which are needed for the calculation of the photoemission intensities.

2.4. Photoemission intensities

The photoemission intensities $I(E, \hbar\omega)$ are calculated in terms of the self-consistent

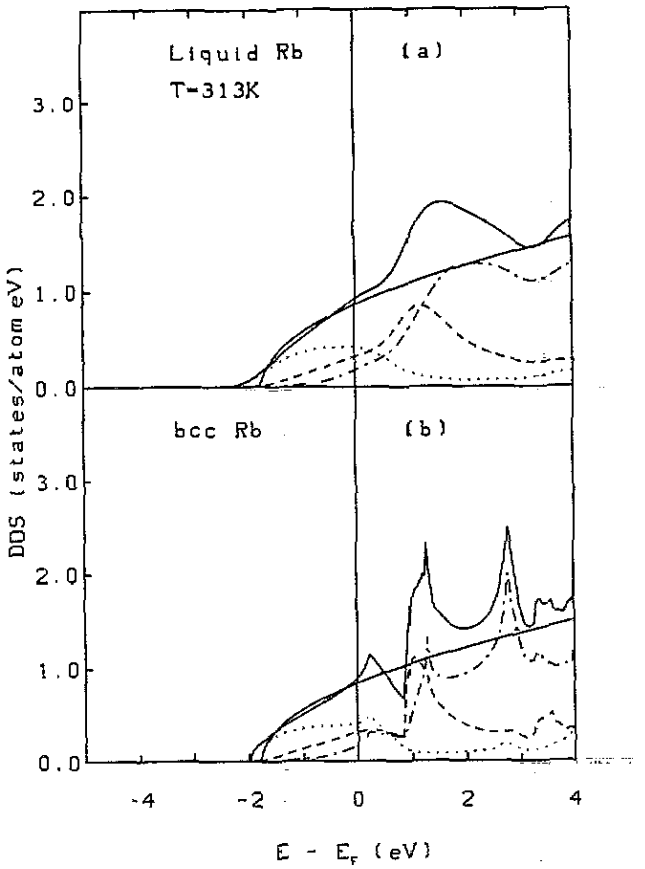

Figure 4. Electronic density of states in liquid Rb at $T = 313$ K (a) and in BCC Rb (b). For key, see figure 3.

potentials and the partial densities of states using the following approximations [35,36]: (a) dipole approximation to the photon field; (b) complete neglect of wavenumber conservation; (c) single-scatterer final-state approximation; (d) independent averages over the directions of the wavevectors of the exciting photon and the emitted electron and over all polarizations.

In fact (b) is an approximation only for crystals. It can be used only at high excitation energies (in x-ray photoemission), where phonon broadening relaxes the condition of wavevector conservation. In the liquid the wavevector is not a conserved quantity and the calculation gives excellent results even for the lower excitation energies of the ultraviolet photoemission spectroscopy (UPS).

3. Results and discussion

The input data for the calculations are summarized in table 1. The interatomic potentials are shown in figure 1. The scaling of distance with the position σ of the first zero and of energy with the depth ϵ of the first minimum demonstrates that the potentials follow approximately a law of corresponding states [37]. Numerical values of ϵ and σ are given in table 2.

Table 1. Input data for the calculations: atomic volume V_c and V_l of the solid and liquid phases and temperatures T of the melts.

	V_c (Å^3)	V_l (Å^3)	T_K
K	75.701	78.610	338
Rb	92.548	96.158	313
Cs	115.794	120.075	303

Table 2. Position σ of first zero and depth ϵ of main minimum in the effective pair potential.

	σ (Å)	ϵ (mRyd)
Li	2.59	4.81
Na	3.12	3.88
K	4.18	1.98
Rb	4.58	1.77
Cs	5.03	1.34

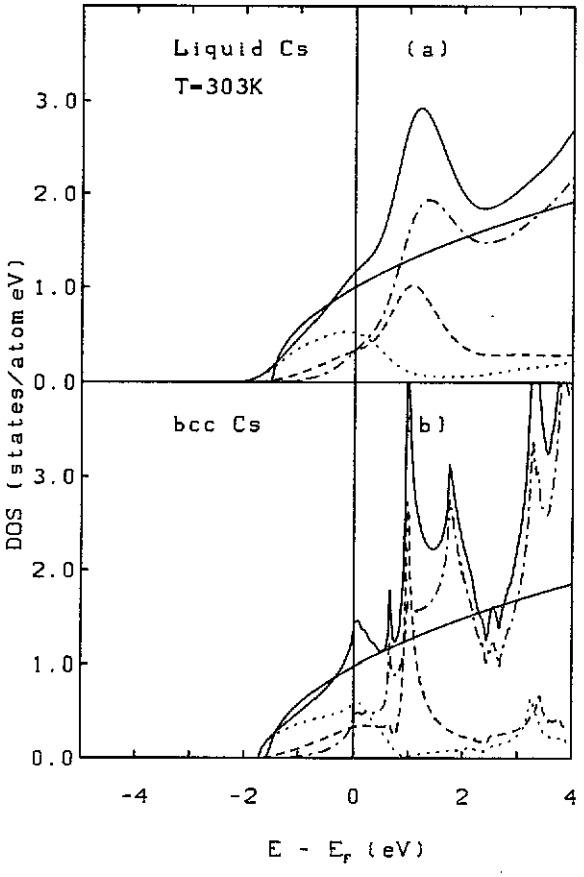

Figure 5. Electronic density of states in liquid Cs at $T = 303$ K (a) and in BCC Cs (b). For key, see figure 3.

Table 3. Fractional s, p, and d charges in the crystalline (c) and liquid (l) metals.

	Z_s		Z_p		Z_d	
	c	l	c	l	c	l
K	0.612	0.621	0.314	0.307	0.074	0.072
Rb	0.633	0.641	0.279	0.275	0.088	0.084
Cs	0.629	0.640	0.244	0.239	0.127	0.121

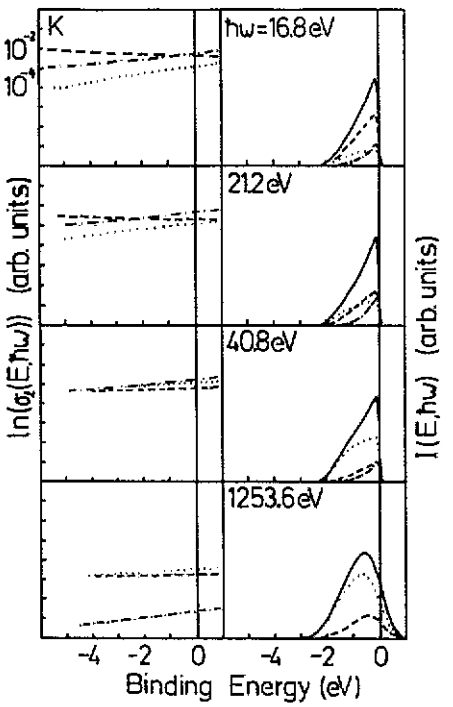

Figure 6. Calculated and measured photoemission intensities $I(E,\hbar\omega)$ and the calculated partial photoionization cross section $\sigma_l(E,\hbar\omega)$ for liquid K at different energies of the exciting photon. Full line: total calculated and experimental photoemission intensity, dotted line: s, dashed line: p and dot-dashed: d electron contribution.

In figure 2 the molecular dynamics result for the static structure factor of the melt close to the freezing point is compared with experiment. Agreement between theory and experiment is very satisfactory, almost to within the experimental uncertainty demonstrated by the comparison of different sets of experimental data [38–40]. The characteristic feature of the structure factor of the liquid heavy alkali metals is the large amplitude of the first peak in $S(q)$ which is even a bit higher than the maximum expected according to Verlet's rule for freezing [41] (maximum $S(Q_p) \sim 2.85$ at melting). This pronounced maximum is a consequence of the strong attractive minimum in the pair potential—see also the analysis of the structure of the liquid alkalis using thermodynamic perturbation theory [42] and integral equation techniques [43].

The electronic densities of states of both the body-centred cubic and the liquid

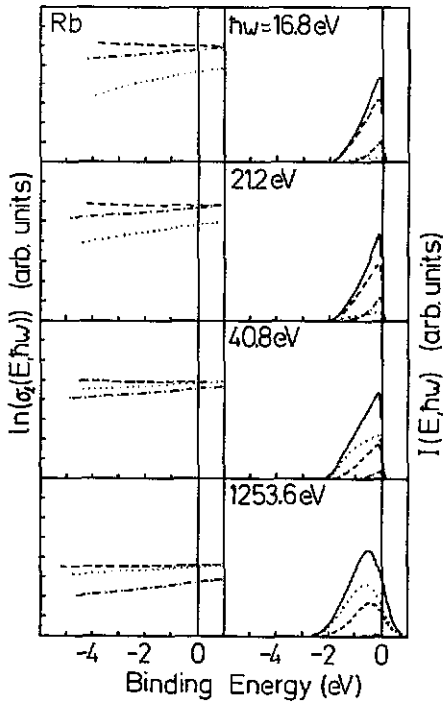

Figure 7. Calculated and measured photoemission intensities $I(E, \hbar\omega)$ and the calculated partial photoionization cross section $\sigma_l(E, \hbar\omega)$ for liquid Rb at different energies of the exciting photon. For key, see figure 6.

metals are reproduced in figures 3 to 5. For the crystalline metals the DOS of the occupied band is rather close to the free electron parabola, but a pronounced peak appears in the empty states at about 1.65 eV (K), 1.3 eV (Rb), and 0.95 eV (Cs) above the Fermi level. The origin of this peak is clearly associated with the onset of the d band and related to the formation of a large band gap at the X-point. The lowering of the d peak relative to the Fermi level in the series K–Rb–Cs parallels a small transfer of electrons from p to d states; the number of s electrons remains almost constant (table 3).

The DOS of the liquid metals is essentially a broadened version of the crystalline DOS. Structural effects are less important in the melt, since the (200) reciprocal lattice vector of the BCC structure associated with the energy gap at the X-point corresponds to a minimum in the static structure factor of the melt. In Rb and Cs the d-electron peak is still well defined and we find the same tendency to a small p–d electron transfer. The broadening of the DOS leads to an even larger overlap of the d band with the occupied part of the band and a markedly non-parabolic (rather triangular) form of the valence band. Very similar effects have been predicted for the heavy alkaline-earth metals Ca, Sr, and Ba [6]. However, in contrast to the case for the alkaline-earth metals where the d-band occupancy is strong enough to induce a pronounced narrowing of the occupied band (we find $Z_d = 0.44$ d electrons in l-Ca, and $Z_d = 0.82$ in l-Ba [6]), the band width of the liquid heavy alkali metals is close to the free electron value.

It should be possible to test the predicted DOS against photoemission experiments.

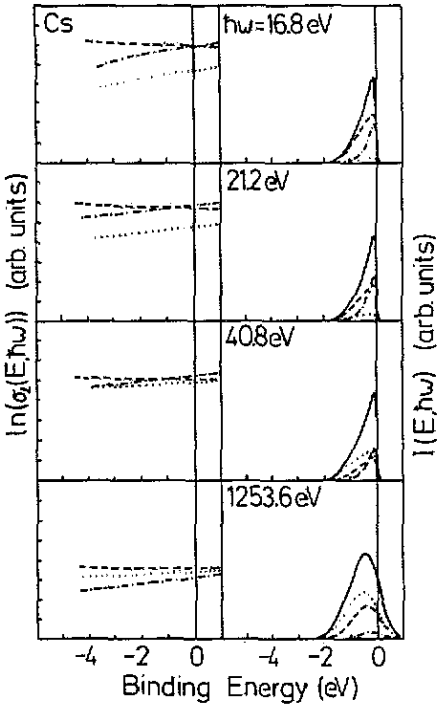

Figure 8. Calculated and measured photoemission intensities $I(E,\hbar\omega)$ and the calculated partial photoionization cross section $\sigma_l(E,\hbar\omega)$ for liquid Cs at different energies of the exciting photon. For key, see figure 6.

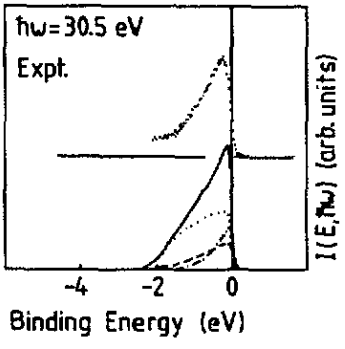

Figure 9. Comparison of measured and calculated photoemission intensity at $\hbar\omega = 30.5$ eV for liquid K. For sake of clarity, the zero of the experimental intensity (after Indlekofer *et al* [4]) has been shifted. For key, see figure 6.

The measured intensity is a weighted average of the partial densities of state, broadened by effects of instrumental resolution (see I for a more detailed discussion). The weighting factors are the partial photoionization cross sections $\sigma_l(E,\hbar\omega)$, which depend on the energy of the exciting photon $\hbar\omega$ and the binding energy of the emitted electron. Our results for a series of photon energies in the UPS and XPS range are compiled in figures 6 to 8. At low photon energies ($\hbar\omega \leqslant 20$ eV), the photoemission intensity is dominated by the p electron DOS, with some contribution from d states in

Rb and Cs and from d and s states in K. This results in a triangular spectrum for l-K ($I(E) \propto (E-E_0)$, where E_0 is the energy corresponding to the bottom of the band), and an almost quadratic energy dependence ($I(E) \propto (E-E_0)^2$) in l-Rb and l-Cs. At the higher photon energies the s-electron contribution to the photoemission spectrum dominates. However, from the much lower experimental resolution ($\sigma \sim 0.5$ eV) and the small band width ($W \leqslant 2$ eV), it is clear that an XPS experiment is not a very sensitive probe of the electronic spectrum of K, Rb, and Cs.

A UPS experiment using a synchrotron source has been performed by Indlekofer *et al* [4]. The comparison between theory and experiment demonstrates perfect agreement (figure 9).

4. Conclusions

This paper completes our investigation of the electronic structure of the liquid alkali metals.

For liquid Li, theory predicts a strong structure-induced modulation of the free-electron DOS and a narrowing of the occupied band. This is fully confirmed by experiment.

For liquid Na and K the calculated DOS is essentially free-electron-like. The difference between the measured quasiparticle band structure and the prediction of local density-functional theory observed for single-crystal spectrums of Na [44] and K [45] does not appear in the electronic spectrum of the melt. Nevertheless, the photoemission spectrum is triangular rather than parabolic, and this is well understood in terms of the partial photoionization cross sections.

For liquid Rb and Cs we predict a measurable deviation of the DOS due to the incipient occupation of the d band. This is reflected in a quadratic energy dependence of the UPS spectrum and we hope that our analysis will stimulate such experiments.

The trends in the calculated DOS at the Fermi level reflect the observed trend in the magnetic susceptibilities: the structure-induced increase in the DOS of l-Li, and the increase in the DOS of l-Rb and l-Cs correlate rather well with the increase of the susceptibility over the free-electron value [46, 47].

Acknowledgments

The numerical calculations were performed on an IBM 3090-400 VF of the Computer Centre of the University of Vienna, supported by the IBM European Academic Supercomputer Initiative (EASI). Financial support form the Fonds zur Förderung der wissenschaftlichen Forschung (Austrian Science Foundation) under project No 7192 is gratefully acknowledged.

References

[1] Oelhafen P, Indlekofer G and Güntherodt H J 1988 *Z. Phys. Chem.* **157** 483
[2] Indlekofer G, Oelhafen P, Lapka R and Güntherodt H J 1988 *Z. Phys. Chem.* **157** 465
[3] Indlekofer G and Oelhafen P 1990 *Proc. 7th Int. Conf. on Liquid and Amorphous Metals (LAM7); J. Non-Cryst. Solids* **117+118** 340
[4] Indlekofer G and Oelhafen P 1990 *1st Liquid Matter Conf., Lyon* unpublished abstracts

[5] Hafner J 1990 *Proc. 7th Int. Conf. on Liquid and Amorphous Metals (LAM7); J. Non-Cryst. Solids* **117+118** 18
[6] Jank W and Hafner J 1990 *Phys. Rev.* B **41** 1497; 1990 *Phys. Rev.* B **42** 6926
[7] Hafner J and Jank W 1990 *Phys. Rev.* B **42** 11530
[8] Jank W and Hafner J 1990 *J. Phys.: Condens. Matter* **2** 5065
[9] Hafner J and Jank W 1991 *Proc. 1st Liquid Matter Conf.; J. Phys.: Condens. Matter* **3** SA239
[10] Cusack N E 1987 *The Physics of Structurally Disordered Materials* (Bristol: Hilger)
[11] Mott N F 1989 *Metal-Insulator Transitions* 2nd edn (London: Taylor and Francis)
[12] Höchst H, Steiner P and Hüfner S 1978 *Z. Phys.* B **30** 145
[13] Takemura K, Minomura S and Shimomura O 1982 *Phys. Rev. Lett.* **49** 1772
[14] Takemura K and Syassen K 1982 *Solid State Commun.* **44** 1161
[15] Takemura K and Syassen K 1983 *Phys. Rev.* B **28** 1193
[16] Olijnyk H and Holzapfel W B 1983 *Phys. Lett.* **99A** 381
[17] Louie S G and Cohen M L 1974 *Phys. Rev.* B **10** 3237
[18] Glötzel D and McMahan A K 1979 *Phys. Rev.* B **20** 3210
[19] Sikka S K 1988 *Phys. Rev.* B **38** 8463
[20] Tsuji K, Yaoita K, Imai M, Mitamura T, Kikegawa T, Shimomura O and Endo H 1990 *Proc. 7th Int. Conf. on Liquid and Amorphous Metals (LAM7); J. Non-Cryst. Solids* **117+118** 72
[21] Heine V and Weaire D 1970 *Solid State Physics* vol 24 (New York: Academic) p 247
[22] Hafner J 1987 *From Hamiltonians to Phase Diagrams (Springer Series in Solid State Sciences 70)* (Berlin: Springer)
[23] Cohen M H and Heine V 1961 *Phys. Rev.* **122** 1821
[24] Vashishta P and Singwi K S 1972 *Phys. Rev.* B **6** 875
[25] Ichimaru S and Utsumi K 1981 *Phys. Rev.* B **24** 7385
[26] Hafner J 1976 *Z. Phys.* B **24** 41
[27] Dacorogna M M and Cohen M L 1986 *Phys. Rev.* B **34** 4996
[28] Skriver H L 1985 *Phys. Rev.* B **31** 1909
[29] Hafner J 1989 *in Cohesion and Structure* vol 2, ed D G Pettifor and F R deBoer (Amsterdam: North-Holland) p 147
[30] Arnold A, Mauser N and Hafner J 1989 *J. Phys.: Condens. Matter* **1** 965
[31] Arnold A and Mauser N 1990 *Comput. Phys. Commun.* **59** 267
[32] Andersen O K, Jepsen O and Glötzel D 1985 *Highlights of Condensed Matter Theory* ed F Bassani, F Fumi and M P Tosi (Amsterdam: North-Holland)
[33] Skriver H L 1984 *The LMTO Method (Springer Series in Solid State Sciences 41)* (Berlin: Springer)
[34] Hafner J and Payne M C 1990 *J. Phys.: Condens. Matter* **2** 221
[35] Jarlborg T and Nilsson P O 1979 *J. Phys. C: Solid State Phys.* **12** 265
[36] Redinger J, Marksteiner P and Weinberger P 1986 *Z. Phys.* B **63** 321
[37] Mountain R D 1977 *Liquid Metals 1976* ed R Evans and D A Greenwood (Bristol: The Institute of Physics) p 62
[38] Huijben M J and van der Lugt W 1979 *Acta Crystallogr.* A **35** 431
[39] Waseda Y 1981 *The Structure of Non-Crystalline Materials—Liquids and Amorphous Solids* (New York: McGraw Hill) p 253
[40] Copley J R D and Lovesey S W 1977 *Liquid Metals 1976 (Inst. Phys. Conf. Ser. 30)* ed R Evans and D A Greenwood (Bristol: Institute of Physics) p 575
[41] Hansen J P and Verlet L 1969 *Phys. Rev.* **184** 151
[42] Kahl G and Hafner J 1985 *Z. Phys.* B **58** 283
[43] Pastore G and Kahl G 1987 *J. Phys. F: Met. Phys.* **17** L267
[44] Lyo I W and Plummer E W 1988 *Phys. Rev. Lett.* **60** 1558
[45] Jensen E, Song K J and Plummer E W unpublished, results quoted in [44]
[46] Kelly P J and Glötzel D 1986 *Phys. Rev.* B **33** 5284
[47] Itami I, Shimoji M, and Shimokawa K 1988 *Z. Phys. Chem.* **157** 587